

Numerical Analysis of Vortex-Induced Yaw Motion of a Paired-Column Semi-Submersible in Currents

Weiwen Zhao, Decheng Wan*

State Key Laboratory of Ocean Engineering, School of Naval Architecture, Ocean and Civil Engineering Shanghai Jiao Tong University, Collaborative Innovation Center for Advanced Ship and Deep-Sea Exploration, Shanghai, China

*Corresponding author: dcwan@sjtu.edu.cn

ABSTRACT

Vortex-induced motions (VIM) is a severe engineering problem for floating structures with slender columns. Moreover, recent studies on VIM of multi-column floating platforms showed that VIM also involves prominent yaw motions. In this paper, numerical simulations of VIM for a paired-column semi-submersible with transverse, inline and yaw degree-of-freedom are performed by our in-house CFD solver naoe-FOAM-SJTU. To avoid mesh distortion induced by yaw motion, a multi-block overset mesh is applied for the fluid domain. In order to accurately predict the flow separation and wake flow, the SST-DDES turbulence model is utilized. Vortex-induced yaw (VIY) is observed during VIM simulations. For high current velocity cases, multi-frequency component for yaw is discovered. The variation of yaw frequencies at different reduced velocities and current headings are discussed. Drag and lift, as well as rotational moment on each column member are analyzed.

1 INTRODUCTION

During last decades, researchers and engineers were devoted to the study of vortex-induced motions of floating offshore structures. As is known to all, the vortex shedding around bluff body will cause alternative pressure changes on both sides as well as back of the body. For floating offshore platforms with vertical column structures, the periodic pressure change is main cause of formation of the vortex-induced motions, or VIM. Previous studies of VIM of Spars^[1] and mono-column^[2] showed that for single-column floating structures, VIM is dominated by transverse (sway) and inline (surge) motions. However, for semi-submersible platforms with multiple columns, the vortex shedding behaviours and frequencies on each column can be different due to the interference between columns under varies current headings. That will consequently results in different oscillating drag and lift forces on each column in terms of frequency, amplitude and phase. This is commonly known as the main reason of yaw motions in VIM for multi-column semi-submersible platforms.

There has been extensive works on the VIM study of semi-submersible platforms both experimentally and numerically. In the very beginning of VIM study of semi-submersible, however, researchers were concentrating on the transverse and inline motion responses of the platform. Yaw motion due to VIM hasn't been discussed too much, see for example, Rijken and Leverette^[3], Hong et al. ^[4]. It was Waals et al. ^[5] who first reported significant yaw motion in their VIM model test of semi-submersible in towing tank. According to their study, the yaw amplitude was up to 6.79 degree for some specific towing direction and pontoon configuration. They conjecture that yaw motion of multi-column floaters induced by current could be due to the galloping phenomenon as the yaw amplitude is not self-limiting but rather increases monotonically with tow speed. In the subsequent experimental studies by Magee et al. ^[6], Gonçalves et al. ^[7,8], Liu et al. ^[9], they also confirmed the yaw motions in VIM for multi-column semi-submersible platforms. As the computational power increases, numerical simulations based on computational fluid dynamics (CFD) method have also

been carried out to the VIM study of semi-submersible platforms. Tan et al. ^[10] simulated the VIM of a multi-column floating platform with commercial CFD software Star-CCM+ and good agreement between model test and CFD simulations were obtained. They found that the yaw motion is sensitive to current headings. The 0 degree current heading gives the largest yaw response. Lee et al. ^[11] performed full-scale and model-scale CFD simulations of VIM response of a deep draft semi-submersible. Transverse, inline and yaw motions are considered in the simulations. Their results showed that the yaw response is also self-limited as transverse motion. The lock-in for yaw however is more complicated than that of transverse motion.

Due to the wake interference contributed by columns and pontoons, VIM characteristics especially the yaw motion for semi-submersible platform is very complicated. Amongst the VIM studies of semi-submersibles which discussed yaw motion characteristics, Liu et al. ^[12] performed both experimental and three-dimensional numerical simulations on the VIM of semi-submersibles. In their study, the yaw motion responses between 0 and 45 degree current headings was distinctly different. The yaw amplitude reached peak value of about 4.5 to 5 degree at 0 degree current heading in the range of non-dimensional reduced velocity from 5 to 8, and decreased sharply. However, the 45 degree current heading case showed the yaw amplitude increase until reduced velocity becomes larger than 8 and then remained at a stable level as reduced velocity continues increasing. To better understanding the yaw characteristics in semi-submersible VIM, the current study performs CFD simulations of a paired-column semi-submersible (PC Semi) platforms with eight columns. Detailed flow field information including three-dimensional vortex structures, as well as force analysis on each individual column will be discussed to reveal the mechanism of yaw motion for multi-column semi-submersibles.

2 MODEL AND DEFINITIONS

The semi-submersible model used in present CFD study is a deep-draft semi-submersible with eight columns. Related model tests have been carried out by Zou et al. ^[13,14] at towing tank in UC Berkley and MARIN with different scale ratio, respectively. The larger model with scale ration 1:54 is adopted in the present study. The model consists of four outer columns and four inner columns with different column sizes. The three-dimensional model of the PC Semi is depicted in Figure 1. Detailed geometric size of the PC Semi can be referred to Zhao et al. ^[15] and will not described here.

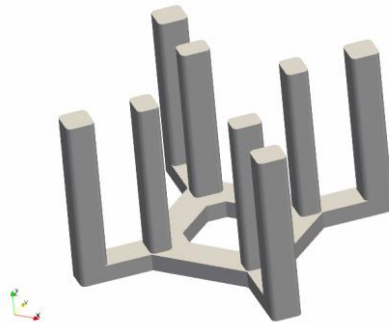


Figure 1: Three-dimensional model of the PC Semi.

The non-dimensioned parameter reduced velocity, U_r , is usually presented in the VIM study to represent the current velocity or towing velocity, which is defined as

$$U_r = \frac{UT_n}{D} \quad (1)$$

where U is the current velocity or towing velocity, T_n is the natural transverse period of the platform under mooring configuration in still water, D is the characteristic diameter of columns. For conventional semi-

submersible with cylinder or square columns, D is the projection diameter perpendicular to current direction. As for PC Semi, D is the diagonal length of the outer column cross section.

For yaw motion analysis, another reduced velocity based on the natural yaw period is usually presented, which is defined as

$$U_{r,yaw} = \frac{UT_{n,yaw}}{D} \quad (2)$$

in which, $T_{n,yaw}$ is the natural yaw period.

When performing analysis on the force and motion characteristics, the lift and drag coefficients, as well as the nominal motion response are introduced. The lift and drag coefficients represent the nondimensional lift forces and drag forces in transverse and inline direction, respectively. They can be expressed as

$$C_L(t) = \frac{F_y(t)}{0.5\rho U^2 A} \quad (3)$$

$$C_D(t) = \frac{F_x(t)}{0.5\rho U^2 A} \quad (4)$$

where ρ is the fluid density, U is the flow velocity, F_y and F_x are hydrodynamic forces act on the platform in the transverse and inline directions, respectively. A is the projected area perpendicular to flow direction.

In addition, the yaw moment coefficient is defined as

$$C_M(t) = \frac{M_z(t)}{0.5\rho U^2 AB} \quad (5)$$

where B is the overall width of the semi-submersible platform.

The motion characteristics of VIM response is defined by the standard deviation of motion amplitude. The nominal transverse and yaw response are defined as:

$$(A_y / D)_{std} = \frac{\sqrt{2}\sigma(A_y(t))}{D} \quad (6)$$

$$(Yaw)_{std} = \sqrt{2}\sigma(yaw(t)) \quad (7)$$

where, σ represents the standard deviation of the transverse or yaw motion time series.

3 NUMERICAL APPROACHES

3.1 CFD solver

The CFD solver naoe-FOAM-SJTU^[15-17] is used for all the simulations throughout this paper. This solver is developed on top of the OpenFOAM framework. It solves the single-phase incompressible flow on a finite volume collocated grid. The coupled pressure and velocity are solved by the segregated PIMPLE method (merged PISO and SIMPLE), in which the standard PISO loop is wrapped by an outer iteration loop with possible under-relaxation of field variables. Differs from the standard PIMPLE family solvers with dynamic motion capabilities in OpenFOAM, naoe-FOAM-SJTU utilizes Euler angle rather than quaternion to describe the motion state and rewrites the six-degree-of-freedom rigid body motion solver combined with the dynamic overset grid capability. The dynamic overset grid is realized by running OpenFOAM flow

solver and overset grid assembler Suggar++^[18] in different processors. For details about the governing equations and solving procedures of the solver, one can refer to Shen et al.^[16] and Zhao et al.^[15].

For turbulence modelling, RANS and DES are available in the current CFD solver. Previous studies^[19,20] compared standard $k-\omega$ SST with DDES model and showed that VIM response obtained by DDES were closer to experimental results. The transverse VIM response of $k-\omega$ SST is slightly larger than DDES. This is due to the excessive eddy viscosity produced by RANS for high Reynolds number flow with strong unsteady separation. For VIM simulations, DES is preferred for turbulence modelling. In this paper, the SST-DDES model is employed for turbulence modelling. SST-DDES^[21] is a “delayed” version of DES, which addresses the “grey area” problems of the original DES model. It can avoid modelled-stress depletion (MSD) which is caused by improper wall-parallel grid spacing in boundary layer. The consequence of MSD, called grid-induced separation (GIS), can also be eliminated.

To deal with large amplitude rigid body motions, the solver applies a six-degrees-of-freedom rigid body motion equation together with the dynamic overset grid. For semi-submersible VIM, the dominant motions are transverse, inline and yaw motions. Therefore in the present VIM study, motions of the semi-submersible platform is obtained by solving the motion equation and is constrained in the horizontal plane. In other words, only transverse, inline and yaw motions are allowed. As for the dynamic grid handling, the overset grid technique can avoid grid distortion and preserve grid quality by moving individual composite grid components freely without mesh deforming.

3.2 Case setup

The computational domain extends to $7B \times 4B \times 3.5T$ (length \times width \times height), in which B is the overall width and T is the draft of the hull, as shown in Figure 2. According to previous studies^[11,22], this domain size is large enough to eliminate the effect of two lateral sides, downstream and bottom.

Figure 3 illustrates the overset grid system used in the present numerical simulations. The unstructured polyhedral overset grid consists of two overlapping mesh blocks: the background mesh in red and the hull mesh in blue. The background mesh is hexahedral with a uniform grid spacing S_b and is generated with the *blockMesh* utility which is a hexahedral mesh generator. The hull mesh is generated by the *snappyHexMesh* utility which is a polyhedral mesh generator based on Cartesian cut-cell approach. The initial base grid size of hull mesh is same as background grid spacing. This ensures all fringe cells could find its corresponding donor cells and avoid orphan cells during overset DCI calculation. Cells in critical region around the hull have been refined up to 4 refinement levels. Ten prism cell layers with expansion ratio of 1.45 are applied to the hull boundary in order to capture boundary layer development. The y^+ for the first layer satisfies $y^+ < 1$ to make sure that the first layer cells are in the viscous sublayer. The final cell numbers in total is 2.43 million.

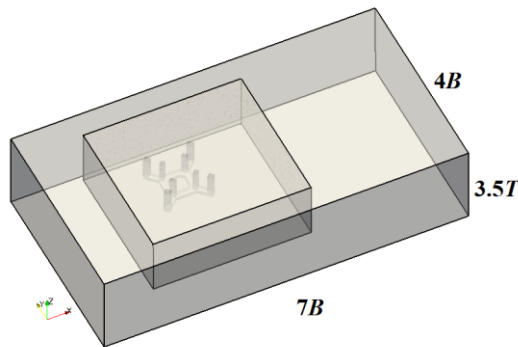


Figure 2: Computational domain.

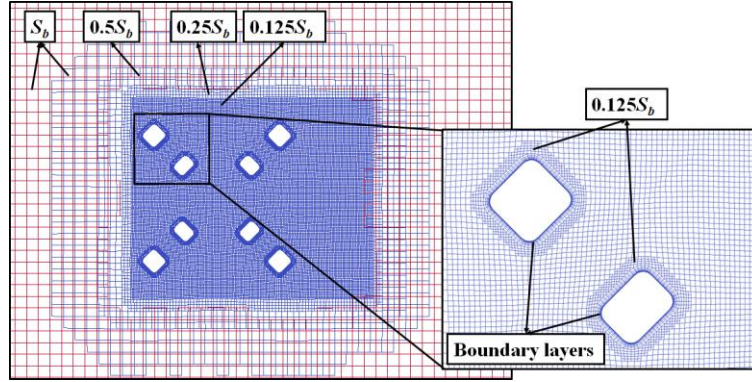


Figure 3: Overset grid system and mesh refinement.

4 RESULTS AND DISCUSSIONS

4.1 Motion responses

Figure 4 presents the results of nominal transverse response at 0 and 45 degree current headings. The hollow markers represent the experimental data from MARIN which is taken from Zou et al.^[14]. The 0 degree cases has more pronounced transverse motion than 45 degree cases. This contradicts with the results of conventional semi-submersible. The reason is the difference of current heading definition between PC Semi and conventional four-column semi-submersible. The current heading definition of conventional semi-submersible is consistent with column flow incident angle. However, for PC Semi the current heading definition is different. E.g., at 0 degree current heading, the column flow incident angle is 45 degree and at 45 degree current heading, columns are parallel with flow direction. It implies that for multi-column floaters with square and rectangular columns, the 45 degree flow incident angle for columns gives the larger transverse VIM response than 0 degree incident angle.

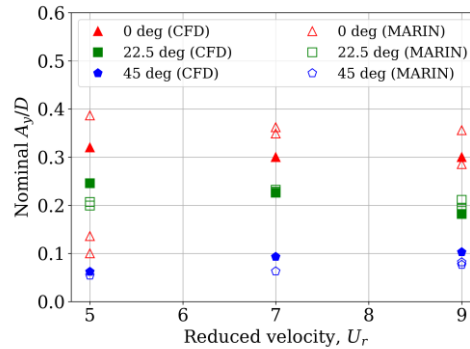


Figure 4: Nominal transverse motion response. Source: Zhao et al.^[23]

Figure 5 shows the spectral analysis of motion response in the transverse direction at different current headings. The 0 degree case gives the strongest transverse motion amplitudes compared with other current headings. Transverse motion frequencies of 0-degree and 22.5-degree current heading at $U_r=5$ is close to the natural transverse frequency f_n , which indicates a resonant behavior on this degree-of-freedom. However, even if the transverse motion frequency is close to the f_n , the transverse motion amplitude is still small for 45-degree heading. It can be attributed to the weak vortex shedding around columns when the column is aligned to incoming flow direction.

The nominal yaw motions, as shown in Figure 6, is different from transverse motions. The 0 degree current heading at $U_r=9$ gives highest yaw response among all cases. Spectral analysis are also performed for yaw motion and the results are given in Figure 7. From the perspective of frequency domain analysis, the yaw motion is more complicated than transverse motion. For high reduced velocities, there are always multiple frequency components excitations that drives the platform rotating at different frequencies. At 0 degree headings, the yaw are dominated by two peak frequencies. For 22.5-degree and 45-degree cases, the dominant yaw frequencies are weaker and the frequency bands are wider.

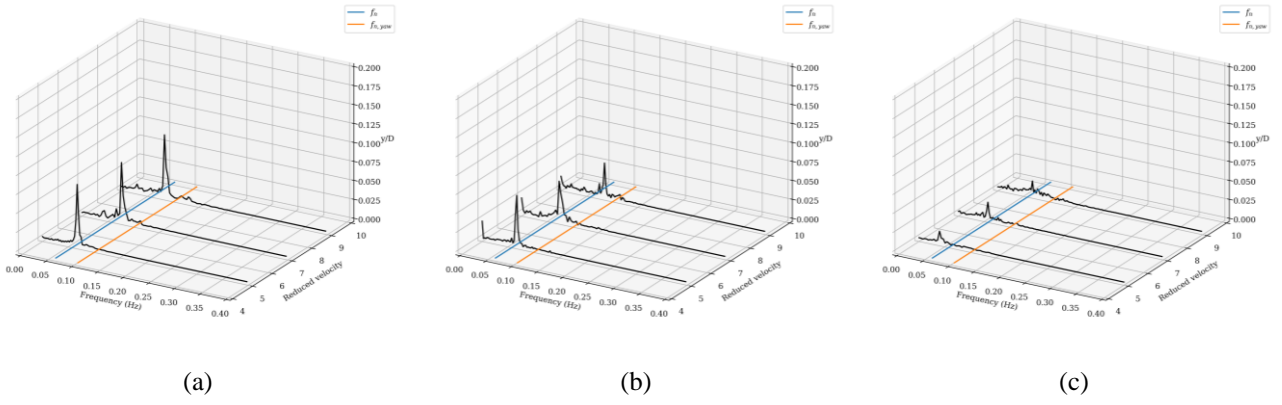


Figure 5: Spectral analysis of transverse motion response at (a) 0 degree, (b) 22.5 degree, (c) 45 degree current headings.

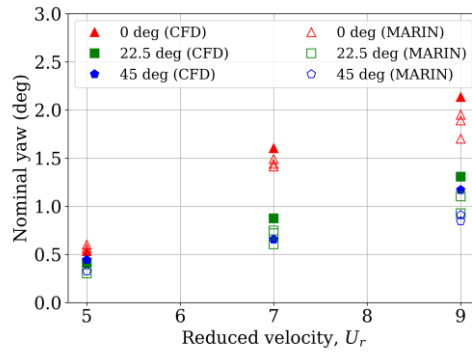


Figure 6: Nominal yaw motion response. Source: Zhao et al. [23]

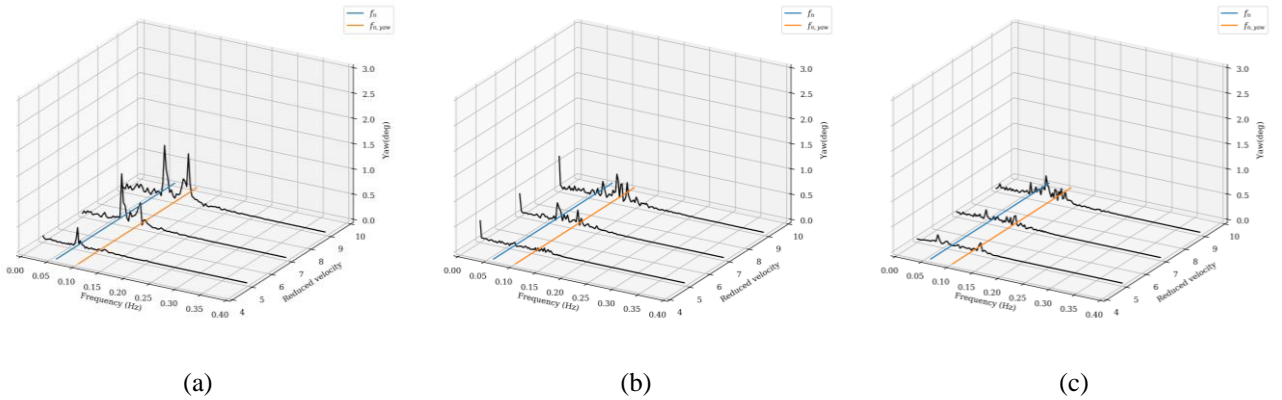


Figure 7: Spectral analysis of yaw motion response at (a) 0-degree, (b) 22.5-degree, (c) 45-degree current headings.

4.2 Forces and Moments Analysis

To better understanding the motion characteristics, the hydrodynamic forces and moments are extracted from the simulation results for further analysis. For simplification, the columns are labelled from OC/IC#1 to OC/IC#4, as shown in Figure 8.

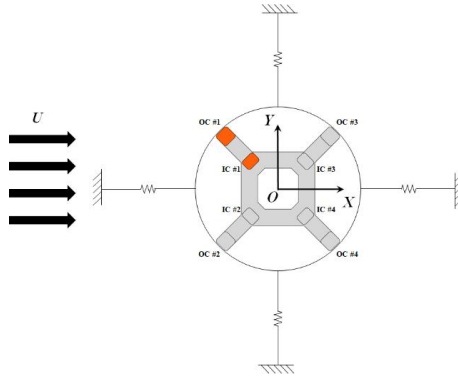


Figure 8: The mooring system and labelling of outer and inner columns for PC Semi.

Figure 9 gives the lift forces on the upstream columns of the PC Semi for 0-degree heading. It can be seen clearly the frequencies and phases for lift forces are highly coincident amongst the four upstream outer and inner columns, OC#1/#2 and IC#1/#2, which indicating a strong synchronization amongst the vortex shedding of upstream columns. When the current heading changes to 22.5 and 45 degrees, the lift forces amplitude decreases compared to 0-degree heading. It's interesting to know that lift force frequencies for upstream columns are all increasing. More importantly, phase shift of lift force exists between any of two columns. The frequency and phase diversity scatter the component of each columns in total lift forces and result in smaller transverse motion responses.

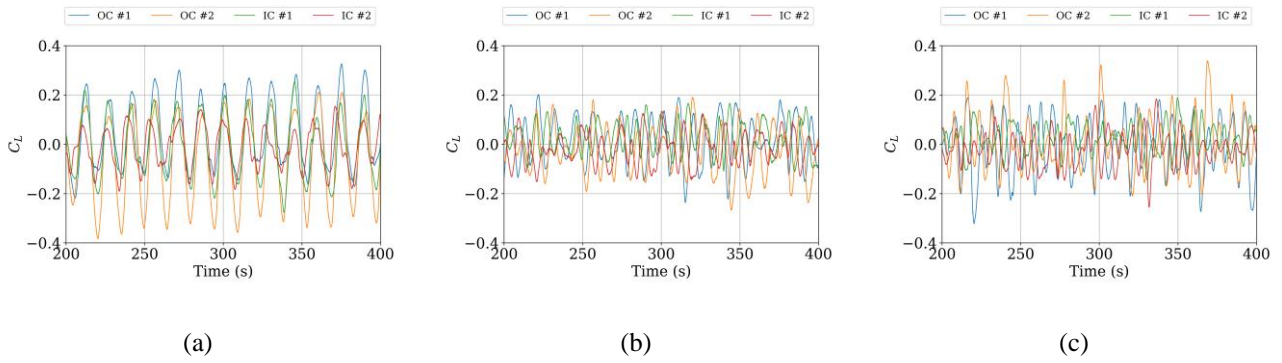


Figure 9: Hydrodynamic lift forces of each upstream columns for 0-degree heading at reduced velocity of (a) $U_r=5$, (b) $U_r=7$, (c) $U_r=9$.

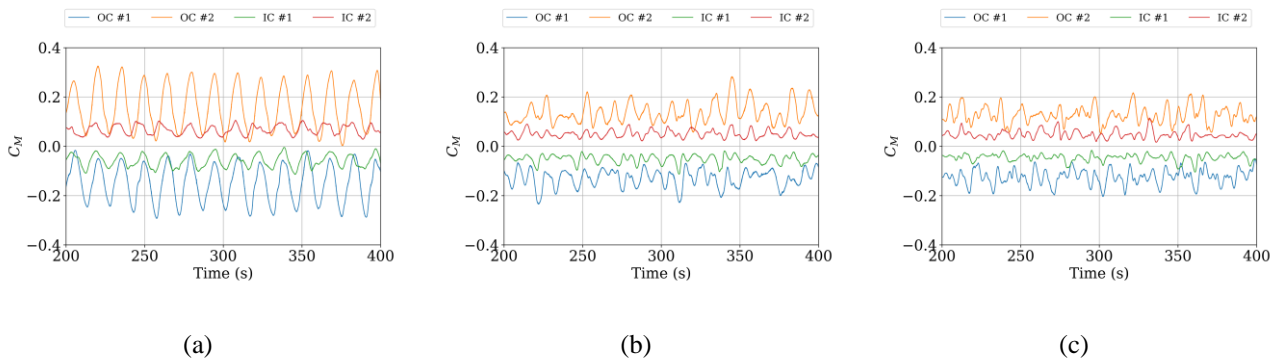


Figure 10: Hydrodynamic yaw moments of each upstream columns for 0-degree heading at reduced velocity of (a) $U_r=5$, (b) $U_r=7$, (c) $U_r=9$.

Figure 10 shows the yaw moment of upstream columns for 0-degree heading at different reduced velocities. A first sight, frequency and phase of yaw moments for upstream columns are similar to lift forces. Phase synchronization exists between upstream columns at reduced velocity $U_r=5$. As reduced velocity

increases to 7 and 9, frequency increases and phase shift occurs. It seems the phase synchronization of moment should amplify the yaw motion response. It is however vice versa, $U_r=5$ gives the smallest yaw response, see Figure 6.

To explain this contradiction, moments on four outer columns are further analysed and presented in Figure 11. The yaw moments on inner columns are omitted due to small contribution to yaw motion. Surprisingly, at $U_r=5$, the phase angle offset between upstream and downstream outer columns is always 180 degree. As a consequence, the total yaw moment is cancelling out and keeps at a small value, which is responsible for the small yaw motion amplitude. For $U_r=7$ and 9 cases, although the time histories of yaw moment are modulated and not as regular as $U_r=5$, there are phase synchronizations between upstream and downstream columns, which contributes to the amplification of yaw motion response.

Figure 11 gives another example of yaw moments for 22.5-degree current heading. The phase shift of yaw moment is also observed at $U_r=5$ in this conditions, but not for high reduced velocities $U_r=7$ and 9. The 45-degree current heading cases show similar phenomenon and will not be presented here.

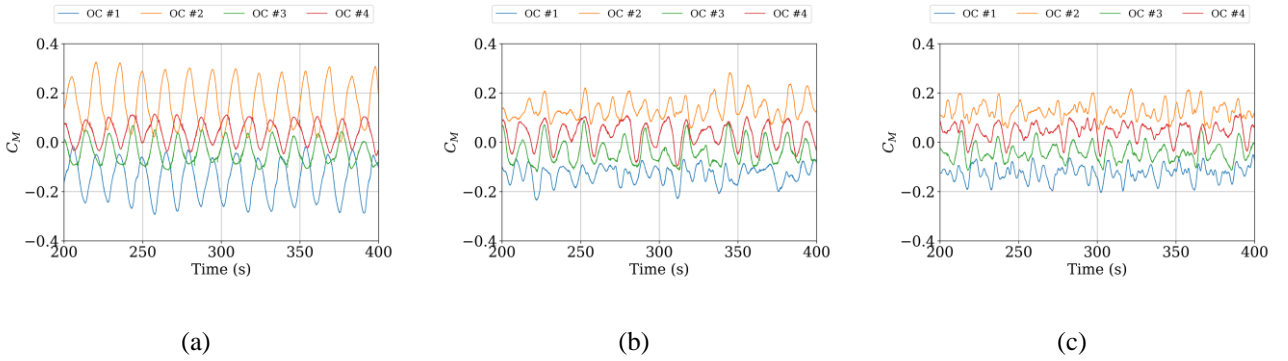


Figure 11: Hydrodynamic yaw moments of each outer columns for 0-degree heading at reduced velocity of (a) $U_r=5$, (b) $U_r=7$, (c) $U_r=9$.

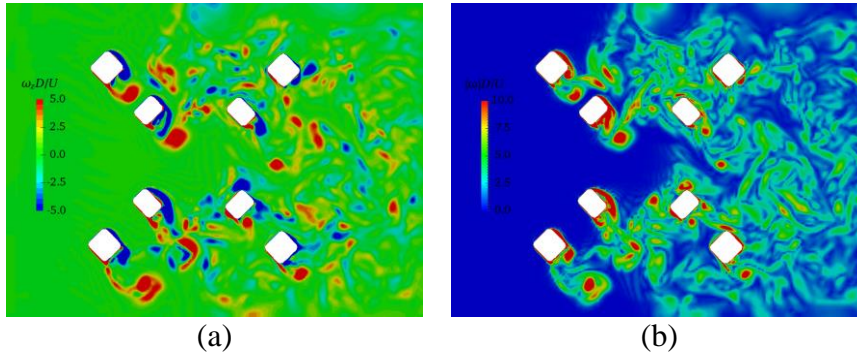


Figure 12: Non-dimensional vorticity contour on the half-draft plane for 0 degree heading at $U_r=5$, coloured by (a) spanwise vorticity, (b) vorticity magnitude.

Figure 12 depicts the vorticity contour on the half-draft plane for 0 degree. The contour are coloured by the non-dimensional spanwise vorticity and vorticity magnitude. The expected synchronization of vortex shedding around the upstream outer and inner columns are observed. In Figure 12(b), some small size eddies occur between upstream and downstream columns, which confirms the three-dimensional effect of vortex shedding from upstream columns. These eddies make the VIM especially yaw motion response more complicated and need to be further studied in the future.

5 CONCLUSION

In this paper, the VIM including transverse, inline and yaw motions of a paired-column semi-submersible are numerically simulated using the naoe-FOAM-SJTU CFD solver. Based on the comparison between CFD and model test results, it is concluded that the present CFD results suit well with experimental

data in terms of statistic values for transverse and yaw motion response. In addition, the following conclusions are drawn:

1. Under 0-degree current heading (45 flow incident angle with respect to column), the PC Semi gives the largest transverse motion amplitude.
2. For 0-degree current heading, transverse force synchronization exists amongst four upstream outer and inner columns.
3. For low reduced velocity $U_r=5$, yaw moment between upstream and downstream columns has a phase angle of 180 degrees.
4. For high reduced velocity $U_r=7$, yaw moment synchronization is observed amongst four outer columns.

ACKNOWLEDGEMENTS

This work is supported by the National Natural Science Foundation of China (51879159, 51490675, 11432009, 51579145), Chang Jiang Scholars Program (T2014099), Shanghai Excellent Academic Leaders Program (17XD1402300), Program for Professor of Special Appointment (Eastern Scholar) at Shanghai Institutions of Higher Learning (2013022), Innovative Special Project of Numerical Tank of Ministry of Industry and Information Technology of China (2016-23/09) and Lloyd's Register Foundation for doctoral student, to which the authors are most grateful.

REFERENCES

- [1] Finnigan, T., Roddier, D. Spar VIM model tests at supercritical reynolds numbers[C]. In Proceedings of the 26th International Conference on Offshore Mechanics and Arctic Engineering. San Diego, California, USA, 2007, **3**: 731–740.
- [2] Gonçalves, R.T., Fajarra, A.L.C., Rosetti, G.F., et al. Mitigation of vortex-induced motion (VIM) on a monocolumn platform: forces and movements[J]. Journal of Offshore Mechanics and Arctic Engineering. 2010, **132**(4): 041102.
- [3] Rijken, O., Leverette, S. Experimental study into vortex induced motion response of semi submersibles with square columns[C]. In Proceedings of the 27th International Conference on Offshore Mechanics and Arctic Engineering. Estoril, Portugal, 2008, **1**: 263–276.
- [4] Hong, Y., Choi, Y., Lee, J., et al. Vortex-induced motion of a deep-draft semi-submersible in current and waves[C]. In Proceedings of the 18th International Offshore and Polar Engineering Conference. Vancouver, British Columbia, Canada, 2008, **3**: 453–459.
- [5] Waals, O.J., Phadke, A.C., Bultema, S. Flow induced motions of multi column floaters[C]. In Proceedings of the 26th International Conference on Offshore Mechanics and Arctic Engineering. San Diego, California, USA, 2007, **1**: 669–678.
- [6] Magee, A., Sheikh, R., Guan, K.Y.H., et al. Model tests for VIM of multi-column floating platforms[C]. In Proceedings of the ASME 30th International Conference on Ocean, Offshore and Arctic Engineering. Rotterdam, The Netherlands, 2011, **7**: 127–136.
- [7] Gonçalves, R.T., Nishimoto, K., Rosetti, G.F., et al. Experimental study on vortex-induced motions (VIM) of a large-volume semi-submersible platform[C]. In Proceedings of the 30th International Conference on Ocean, Offshore and Arctic Engineering. Rotterdam, The Netherlands, 2011, **7**: 1–9.
- [8] Gonçalves, R.T., Rosetti, G.F., Fajarra, C., et al. Vortex-induced yaw motion (VIY) of a large-volume semi-submersible platform[C]. In Proceedings of the 22nd International Offshore and Polar Engineering Conference. Rhodes, Greece, 2012, **3**: 572–578.
- [9] Liu, M., Xiao, L., Lu, H., et al. Experimental study on vortex-induced motions of a semi-submersible with square columns and pontoons at different draft conditions and current incidences[J]. International Journal of Naval Architecture and Ocean Engineering. 2017, **9**(3): 326–338.
- [10] Tan, J.H.C., Magee, A., Kim, J.W., et al. CFD simulation for vortex induced motions of a multi-column floating platform[C]. In Proceedings of the 32nd International Conference on Ocean, Offshore and Arctic Engineering. Nantes, France, 2013, **7**: V007T08A066.
- [11] Lee, S.-K., Chien, H.-P., Gu, H. CFD study of deep draft semisubmersible VIM[C]. In Proceedings of the Offshore Technology Conference-Asia. Kuala Lumpur, Malaysia, 2014.
- [12] Liu, M., Xiao, L., Liang, Y., et al. Experimental and numerical studies of the pontoon effect on vortex-induced motions of deep-draft semi-submersibles[J]. Journal of Fluids and Structures. 2017, **72**: 59–79.

- [13] Zou, J., Poll, P., Roddier, D., et al. VIM testing of a paired column semi submersible[C]. In Proceedings of the ASME 32nd International Conference on Ocean, Offshore and Arctic Engineering. Nantes, France, 2013, **7**: V007T08A001.
- [14] Zou, J., Poll, P., Antony, A., et al. VIM model testing and VIM induced mooring fatigue of a dry paired-column semisubmersible platform[C]. In Proceedings of the Offshore Technology Conference. Houston, Texas, USA, 2014.
- [15] Zhao, W., Zou, L., Wan, D.C., et al. Numerical investigation of vortex-induced motions of a paired-column semi-submersible in currents[J]. *Ocean Engineering*. 2018, **164**: 272–283.
- [16] Shen, Z., Wan, D.C., Carrica, P.M. Dynamic overset grids in OpenFOAM with application to KCS self-propulsion and maneuvering[J]. *Ocean Engineering*. 2015, **108**: 287–306.
- [17] Wang, J., Zou, L., Wan, D.C. CFD simulations of free running ship under course keeping control[J]. *Ocean Engineering*. 2017, **141**: 450–464.
- [18] Noack, R.W., Boger, D.A., Kunz, R.F., et al. Suggar++: An improved general overset grid assembly capability[C]. In 19th AIAA Computational Fluid Dynamics Conference. San Antonio, Texas, USA, 2009.
- [19] Kim, S.J., Spornjak, D., Holmes, S., et al. Vortex-induced motion of floating structures: CFD sensitivity considerations of turbulence model and mesh refinement[C]. In Proceedings of the 34th International Conference on Ocean, Offshore and Arctic Engineering. St. John's, Newfoundland, Canada, 2015, **2**: V002T08A057.
- [20] Vinayan, V., Antony, A., Halkyard, J., et al. Vortex-induced motion of deep-draft semisubmersibles: A CFD-based parametric study[C]. In Proceedings of the 34th International Conference on Ocean, Offshore and Arctic Engineering. St. John's, Newfoundland, Canada, 2015, **2**: V002T08A003.
- [21] Gritskevich, M.S., Garbaruk, A.V., Schütze, J., et al. Development of DDES and IDDES formulations for the $k-\omega$ shear stress transport model[J]. *Flow, Turbulence and Combustion*. 2011, **88**(3): 431–449.
- [22] Liang, Y., Tao, L. Interaction of vortex shedding processes on flow over a deep-draft semi-submersible[J]. *Ocean Engineering*. 2017, **141**: 427–449.
- [23] Zhao, W., Wan, D.C., Chen, G. Vortex shedding and its impacts on the motions of a paired-column semi-submersible[C]. In Proceedings of the 28th International Offshore and Polar Engineering Conference. Sapporo, Japan, 2018, **3**: 916–923.